

# 7 WSR-88D OBSERVATIONS OF AN EXTREME HAIL EVENT IMPACTING ABILENE, TX ON 12 JUNE 2014

ARTHUR WITT\*

*NOAA/National Severe Storms Laboratory, Norman, OK*

MIKE JOHNSON

*NOAA/National Weather Service, Memphis, TN*

## 1. INTRODUCTION

On 12 June 2014, an intense supercell thunderstorm with hail to at least 12 cm in diameter (Fig. 1) impacted Abilene, Texas, during the Children’s Art and Literacy festival and parade, resulting in several minor injuries. The storm produced widespread damage to vehicles, homes, and businesses, costing an estimated 400 million dollars. More than 200 city vehicles sustained significant damage, with Abilene Fire Station #4 rendered uninhabitable. Given the storm’s path over a fairly high population-density area, an impressive ground-truth data set of surface hail observations was collected on this event. This included a combination of reports from the National Severe Storms Laboratory’s Severe Hazards Analysis and Verification Experiment (SHAVE; (Ortega et al. 2009)), and from the National Weather Service (NWS) office in San Angelo, TX. The resulting data set included 38 observations of hail  $\geq 70$  mm, 25 observations of hail 51–64 mm, and 22 observations of hail 18–44 mm in diameter (85 total observations of hail  $\geq 18$  mm). This study examined the character and evolution of the Abilene hailstorm from 2100–2359 UTC (hereafter all times are in UTC), as seen by the KDYX WSR-88D, in terms of overall storm intensity, along with the low-altitude dual-polarization (DP) observations associated with the 85 large hail reports.

## 2. DATA AND METHODS

### a. Hailstone observations

Of the 85 observations of large hail for this event, 46 were obtained via the SHAVE project, and 39 from additional reports collected by the NWS. All hail observations



FIG. 1. Pictures of two huge hailstones from the Abilene supercell.

included information on the maximum hail size and location of the report. The time of the hail observation was also available for all the SHAVE reports and 11 of the NWS reports. However, most of these report times did not match (within several minutes) the radar-based time for when the storm core passed over the location of the report (this is a well-known problem; Witt et al. 1998b; Blair et al. 2011). We therefore determined, for each of the 85 hail observations, a best radar-based estimate for the time when the hail observation most likely occurred.

### b. Radar-based parameters

Storm intensity was assessed via five radar parameters. The two velocity-based parameters were derived from the radial velocity data, with the three reflectivity-based parameters determined after “mapping” the radial reflectivity data to a 3D latitude-longitude-height grid at a resolution of  $0.01^\circ \times 0.01^\circ \times 1.0$  km (Lakshmanan et al. 2006). The three reflectivity-based parameters examined were the

\*Corresponding author address: Arthur Witt, NOAA/National Severe Storms Laboratory, 120 David L. Boren Blvd., Norman, OK, 73072.

E-mail: Arthur.Witt@noaa.gov

maximum reflectivity at the  $-20^{\circ}\text{C}$  height ( $Z_{253K}$ )<sup>1</sup>, vertically integrated liquid water content (VIL; Amburn and Wolf 1997), and maximum expected size of hail (MESH; Witt et al. 1998a; Lakshmanan et al. 2007). The two velocity-based parameters examined were the maximum storm-top divergent outflow (STD; Witt and Nelson 1991) and maximum mid-altitude rotational velocity (MRV; Witt 1998). The STD and MRV were calculated as:

$$STD = V_{max} - V_{min} \quad (1)$$

$$MRV = (V_{max} - V_{min})/2 \quad (2)$$

where  $V_{min}$  and  $V_{max}$  are the peak inbound and outbound velocities in the storm's divergence and rotation signatures. To minimize errors in the measurement of STD and MRV, only radial velocity data with corresponding reflectivity  $\geq 15$  dBZ and spectrum width  $< 13$   $\text{m s}^{-1}$  were used. An additional criterion, to avoid use of unreliable data, was that a candidate velocity have sufficient spatial continuity with neighboring velocities on the same elevation scan, defined here as at least one adjacent velocity value within  $5$   $\text{m s}^{-1}$  of the candidate velocity value.

The low-altitude DP data above the locations of the hail reports were also examined as the storm passed over these locations. The DP data analyzed included the reflectivity ( $Z$ ), differential reflectivity ( $Z_{DR}$ ), co-polar correlation coefficient ( $\rho_{HV}$ ) and specific differential phase ( $K_{DP}$ ) (see Kumjian 2013, for a description of the polarimetric radar variables). Measures of these variables on the lowest elevation scan ( $0.52^{\circ}$ ) were calculated using the median value of the eight radar bins within a  $1^{\circ} \times 1$  km window centered on the location of the hail report. Given an update rate of 3–5 min for the lowest elevation scan (KDYX was scanning in Volume Coverage Pattern 212), it was often necessary to extrapolate the position of the  $1^{\circ} \times 1$  km window based on storm motion to the closest scan, in time, to when the storm core passed over the location of the hail report. Also examined was the hail differential reflectivity ( $H_{DR}$ ), defined by Aydin et al. (1986) as:

$$H_{DR} = Z - f(Z_{DR}), \quad (3)$$

where

$$f(Z_{DR}) = \begin{cases} 27 & (Z_{DR} \leq 0 \text{ dB}), \\ 19Z_{DR} + 27 & (0 \leq Z_{DR} \leq 1.74 \text{ dB}), \\ 60 & (Z_{DR} \geq 1.74 \text{ dB}). \end{cases}$$

The  $H_{DR}$  was developed to distinguish hail versus rain.

<sup>1</sup>The  $-20^{\circ}\text{C}$  height was selected based on this being an important temperature for the growth of large hail (Nelson 1983).

### 3. RADAR OBSERVATIONS

#### a. Character and evolution of storm intensity

The Abilene hailstorm began via the merging of a newly developing cell on the west side of a strong multicellular storm  $\sim 2100$ , after which the storm evolved into a more classic supercell by  $\sim 2130$  (Fig. 2). The storm then maintained supercell characteristics for the remainder of the time period examined. In terms of the reflectivity-based parameters examined (Fig. 3), the  $Z_{253K}$  was already quite high at  $\sim 60$  dBZ at 2107, with the VIL and MESH at more modest intensity levels, typical of marginally-severe multicell storms. As the Abilene hailstorm evolved into a supercell over the next 30 min, the VIL and MESH both increased significantly (by 2–3 times their value at 2107), before ultimately reaching peak values later in the time period.

As the storm progressed southeastward toward Abilene, a rapid increase in MESH occurred  $\sim 2155$ , to a maximum of 113 mm, followed by a rapid decrease to 63 mm at 2202 (Fig. 3). This maximum value in MESH occurred  $\sim 1$  hr prior to several reports of softball-size hail (114 mm). The decrease in MESH was short-lived ( $\sim 10$  min), with a second relative maximum of 92 mm at 2208. A notable weakening in storm intensity then occurred, with a decrease to 42 mm at 2223. The storm then strengthened again, with MESH generally in the range of 60–95 mm until 2319. After 2319, there was a more sustained weakening to a range of  $\sim 30$ –50 mm, as the storm moved southeast of Abilene. With the exception of the brief, but large, spike in MESH  $\sim 2155$ , the VIL generally followed the same pattern as MESH over the time period, but with smaller variations in magnitude. The  $Z_{253K}$  showed the smallest variations, mostly staying between  $\sim 60$ –70 dBZ.

Although the rate of increase wasn't as rapid for the STD compared to MESH or VIL, it did nearly double in magnitude between 2107 and 2206, reaching a relative maximum of  $92$   $\text{m s}^{-1}$  (Fig. 4). From 2206 to 2252, when the STD reached a maximum of  $102$   $\text{m s}^{-1}$ , STD followed the same pattern as MESH. However, unlike the MESH, which continued to slowly increase to a secondary maximum of 95 mm at 2310, the STD began generally weakening after 2252, before increasing again to a relative maximum of  $88$   $\text{m s}^{-1}$  at 2330. The MRV displayed much less variation in magnitude, slowly increasing from  $18$   $\text{m s}^{-1}$  at 2107 to a maximum of  $34$   $\text{m s}^{-1}$  at 2210. It then remained within a range of 21–32  $\text{m s}^{-1}$  for the rest of the time period analyzed.

#### b. Low-altitude dual-polarization observations

Two aspects of the relationship between the low-altitude DP observations and the hail reports were explored: 1) the overall distribution of the DP observations for the whole

set of hail reports, and 2) the extent to which these parameters could discriminate between three hail-size ranges: 18–44 mm, 51–64 mm and  $\geq 70$  mm. In terms of individual DP parameters, the results show that most of the large hail was associated with high  $Z$  ( $> 55$  dBZ) (Fig. 5), low  $Z_{DR}$  ( $< 2$  dB) (Fig. 6) and a fairly wide range of  $\rho_{HV}$  (0.9–1.00) (Fig. 7),  $H_{DR}$  (0–40) (Fig. 8) and  $K_{DP}$  (0–5° km<sup>-1</sup>) (Fig. 9). The degree of hail-size discrimination was best for  $H_{DR}$  (Fig. 8) and  $Z_{DR}$  (Fig. 6), with little or no difference seen in  $Z$  (Fig. 5),  $\rho_{HV}$  (Fig. 7) and  $K_{DP}$  (Fig. 9).

We also investigated the degree of hail-size discrimination for six pairs of DP parameters (as previously done by Picca and Ryzhkov (2012); see their Fig. 11). The best apparent hail-size discrimination involved  $Z_{DR}$ -based pairs, namely  $Z$ - $Z_{DR}$  (Fig. 10),  $Z_{DR}$ - $H_{DR}$  (Fig. 11) and  $Z_{DR}$ - $K_{DP}$  (Fig. 12). This is not surprising, given that  $Z_{DR}$  and  $H_{DR}$  (which is a function of  $Z_{DR}$ ) were the best individual DP parameters at discriminating between the three hail-size ranges. No discrimination was evident in  $Z$ - $\rho_{HV}$  (Fig. 13) or  $Z_{DR}$ - $\rho_{HV}$  (Fig. 14), with perhaps a small degree of discrimination in  $Z$ - $K_{DP}$  (Fig. 15).

#### 4. CONCLUSIONS

The damage potential and threat to life and property associated with a severe storm increases at a nonlinear rate as the intensity of the storm increases. Hence, timely identification and warning on the occurrence of extreme severe-weather events, such as the very-large, damaging hail produced by the Abilene supercell, is vital. In that regard, the MESH did an excellent job at predicting the hail threat via a peak value of 113 mm around an hour prior to several softball-size (114 mm) hail observations. The STD briefly exceeded 100 m s<sup>-1</sup> (maximum STD of 102 m s<sup>-1</sup>) within several minutes of the softball-size hail observations, with the MRV occasionally exceeding 30 m s<sup>-1</sup> between 20–40 min prior to the maximum in STD.

The low-altitude DP observations associated with the 85 hail reports showed that most of the large hail occurred in areas of  $Z > 55$  dBZ and  $Z_{DR} < 2$  dB, with the other DP parameters having a fairly wide range of values. Subdividing the hail observations into three size ranges showed that the  $H_{DR}$  and  $Z_{DR}$  had the best hail-size discrimination ability. In terms of paired DP parameters, the results showed the best hail-size discrimination ability for  $Z$ - $Z_{DR}$ ,  $Z_{DR}$ - $H_{DR}$  and  $Z_{DR}$ - $K_{DP}$ .

#### References

- Amburn, S. A., and P. L. Wolf, 1997: VIL density as a hail indicator. *Wea. Forecasting.*, **12**, 473–478, doi:10.1175/1520-0434(1997)012<0473:VDAABI>2.0.CO;2.
- Aydin, K., T. A. Seliga, and V. Balaji, 1986: Remote sensing of hail with a dual-linear polarization radar. *J. Climate Appl. Meteor.*, **25**, 1475–1484, doi:10.1175/1520-0450(1986)025<1475:RSOHW>2.0.CO;2.
- Blair, S. F., D. R. Deroche, J. M. Boustead, J. W. Leighton, B. L. Barjenbruch, and W. P. Gargan, 2011: A radar-based assessment of the detectability of giant hail. *E-Journal of Severe Storms Meteorology*, **6** (7), 1–30, [Available online at <http://www.ejssm.org/ojs/index.php/ejssm/article/view/87>].
- Kumjian, M. R., 2013: Principles and applications of dual-polarization weather radar. Part I: Description of the polarimetric radar variables. *J. Operational Meteor.*, **1** (19), 226–242, doi:10.15191/nwajom.2013.0119.
- Lakshmanan, V., T. Smith, K. Hondl, G. J. Stumpf, and A. Witt, 2006: A real-time, three-dimensional, rapidly updating, heterogeneous radar merger technique for reflectivity, velocity, and derived products. *Wea. Forecasting.*, **21**, 802–823, doi:10.1175/WAF942.1.
- Lakshmanan, V., T. Smith, G. Stumpf, and K. Hondl, 2007: The Warning Decision Support System – Integrated Information. *Wea. Forecasting.*, **22**, 596–612, doi:10.1175/WAF1009.1.
- Nelson, S. P., 1983: The influence of storm flow structure on hail growth. *J. Atmos. Sci.*, **40**, 1965–1983, doi:10.1175/1520-0469(1983)040%3C1965:TIOSFS%3E2.0.CO;2.
- Ortega, K., T. Smith, K. Manross, A. Kolodziej, K. Scharfenberg, A. Witt, and J. Gourley, 2009: The severe hazards analysis and verification experiment. *Bull. Amer. Meteor. Soc.*, **90**, 1519–1530, doi:10.1175/2009BAMS2815.1.
- Picca, J., and A. Ryzhkov, 2012: A dual-wavelength polarimetric analysis of the 16 May 2010 Oklahoma City extreme hailstorm. *Mon. Wea. Rev.*, **140**, 1385–1403, doi:10.1175/MWR-D-11-00112.1.
- Witt, A., 1998: The relationship between WSR-88D measured midaltitude rotation and maximum hail size. Preprints, *19th Conference on Severe Local Storms*, Minneapolis, MN, Amer. Meteor. Soc., 740–743.
- Witt, A., M. D. Eilts, G. J. Stumpf, J. T. Johnson, E. D. W. Mitchell, and K. W. Thomas, 1998a: An enhanced hail detection algorithm for the WSR-88D. *Wea. Forecasting.*, **13**, 286–303, doi:10.1175/1520-0434(1998)013<0286:AEHDAF>2.0.CO;2.
- Witt, A., M. D. Eilts, G. J. Stumpf, E. D. W. Mitchell, J. T. Johnson, and K. W. Thomas, 1998b: Evaluating the performance of WSR-88D severe storm detection algorithms. *Wea. Forecasting.*, **13**, 513–518, doi:10.1175/1520-0434(1998)013<0513:ETPOWS>2.0.CO;2.
- Witt, A., and S. P. Nelson, 1991: The use of single-Doppler radar for estimating maximum hailstone size. *J. Appl. Meteor.*, **30**, 425–431, doi:10.1175/1520-0450(1991)030<0425:TUOSDR>2.0.CO;2.

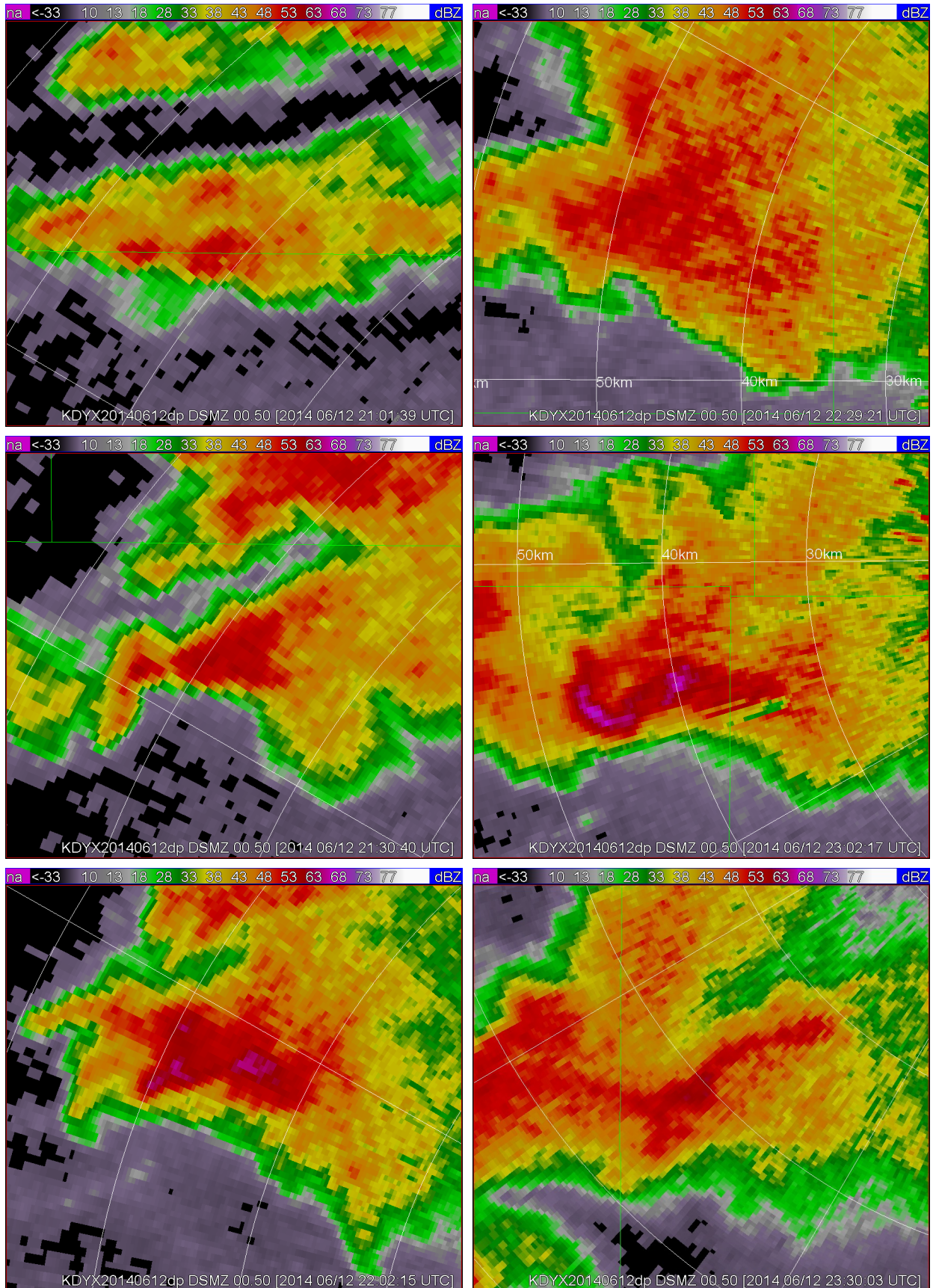


FIG. 2. Reflectivity images from the 0.52° scan at ~30 min intervals. The center of Abilene is located ~ 255° and 45 km from KDYX.

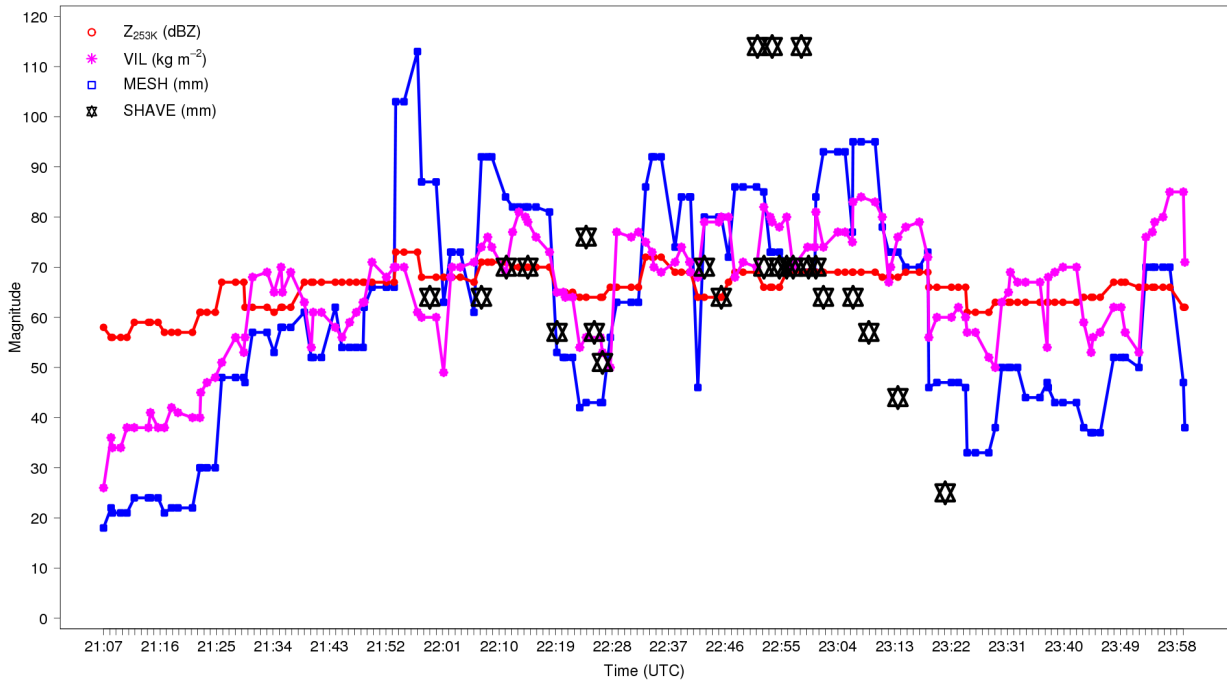


FIG. 3. Time series of  $Z_{253K}$ , VIL and MESH for the Abilene hailstorm. Also shown are the maximum hail sizes from the SHAVE reports.

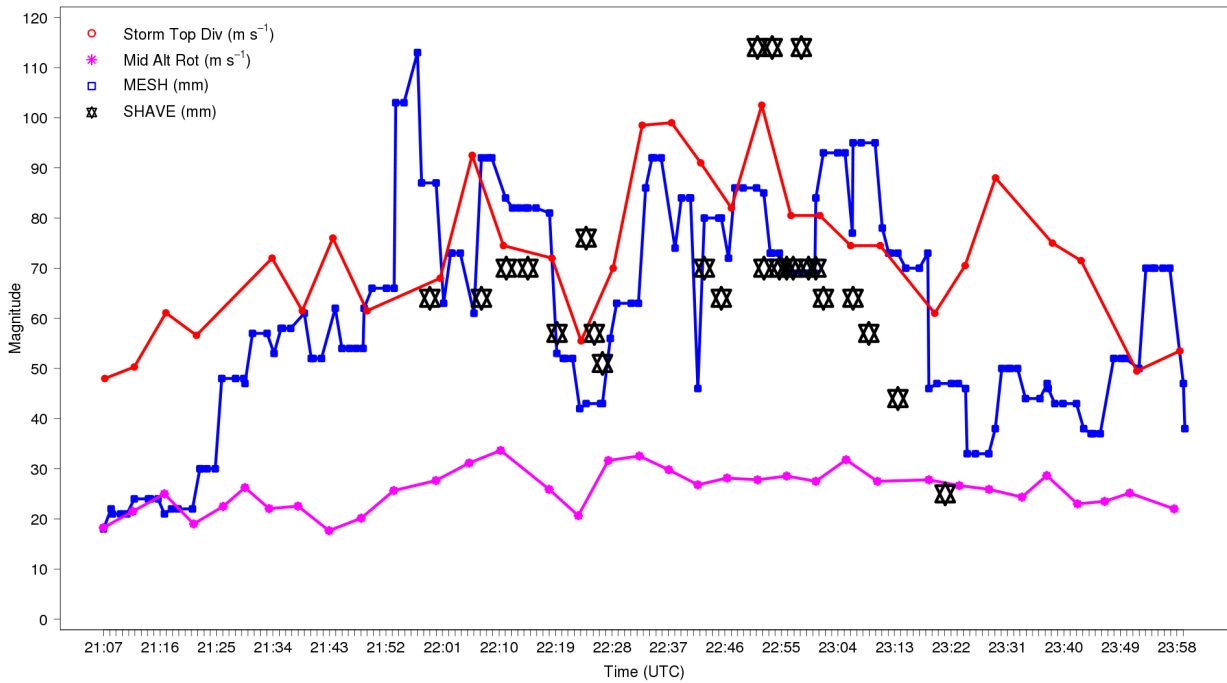


FIG. 4. Same as Fig. 3, except for STD, MRV and MESH.

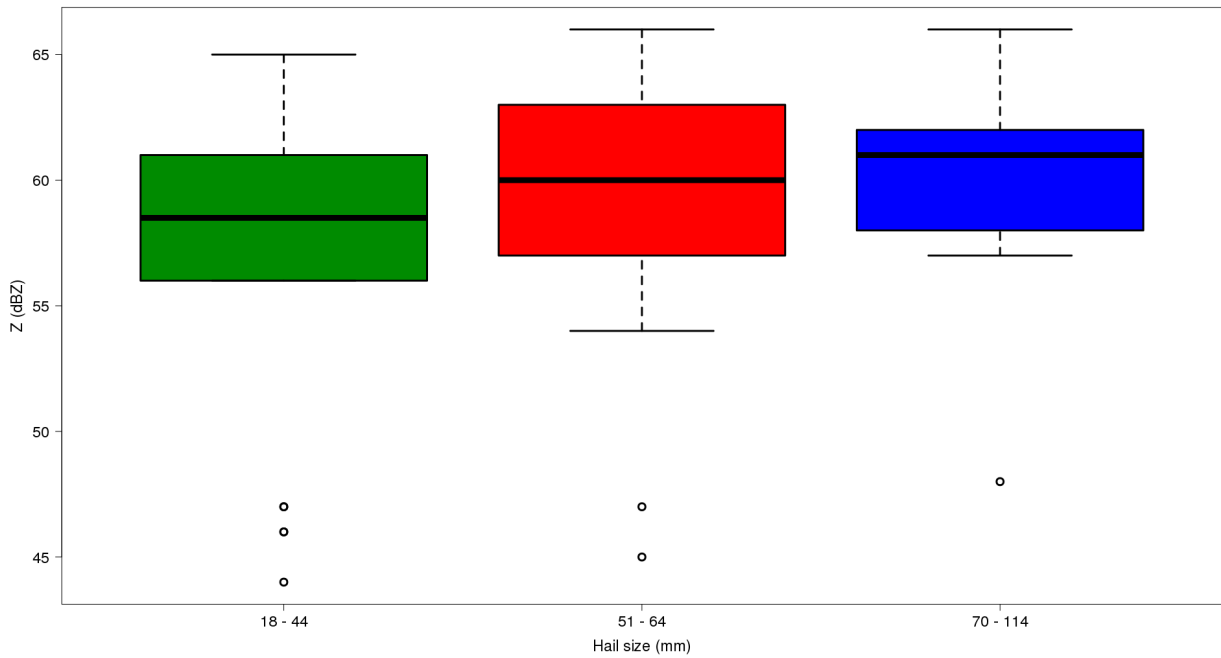


FIG. 5. Box plot of Z from the  $0.52^\circ$  scan for a  $1^\circ \times 1$  km window (median of eight values) centered on the location of each hail report, for three hail-size ranges.

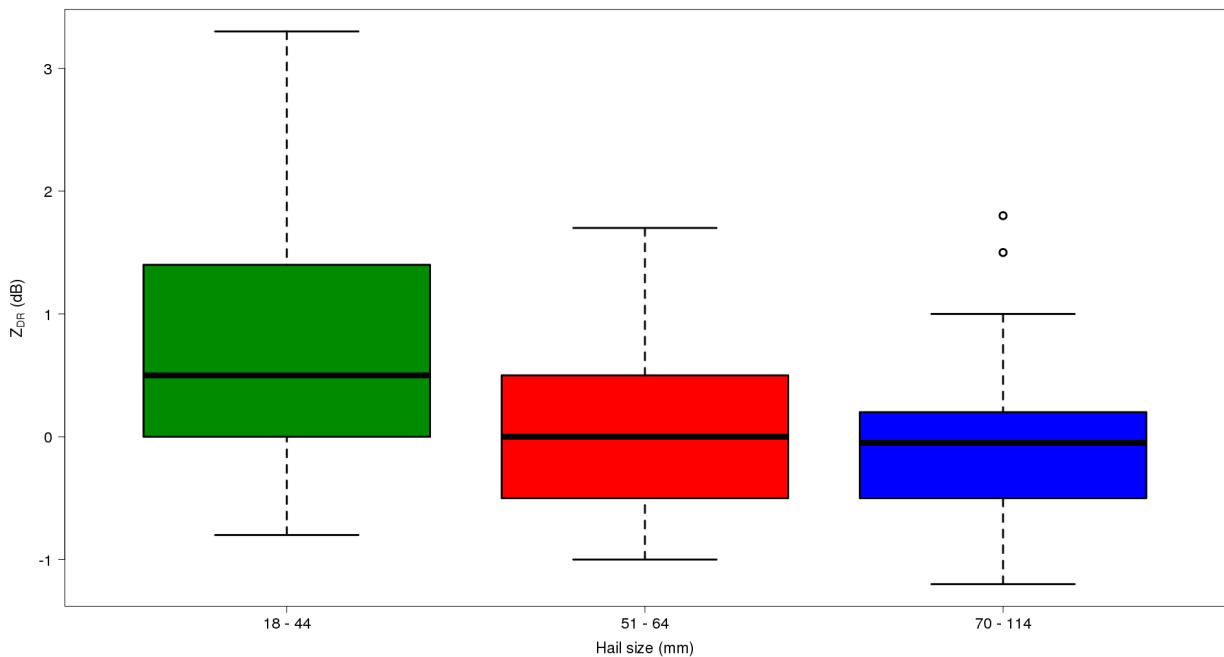


FIG. 6. Same as Fig. 5, except for Z<sub>DR</sub>.

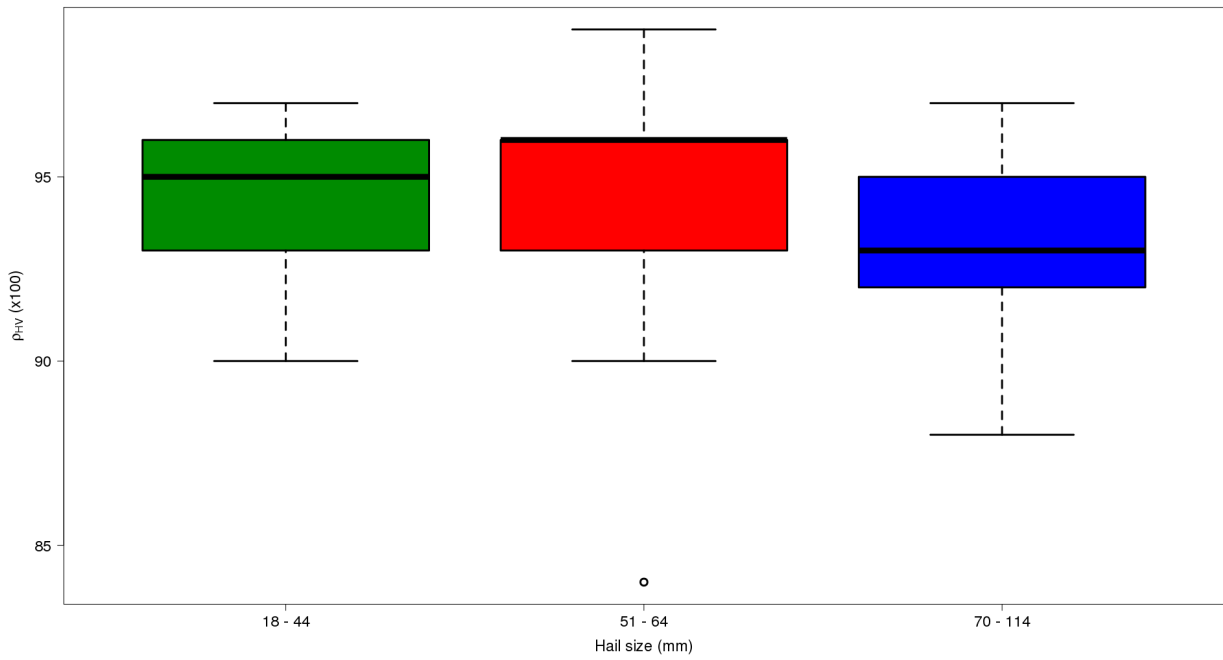


FIG. 7. Same as Fig. 5, except for  $\rho_{HV}$ .

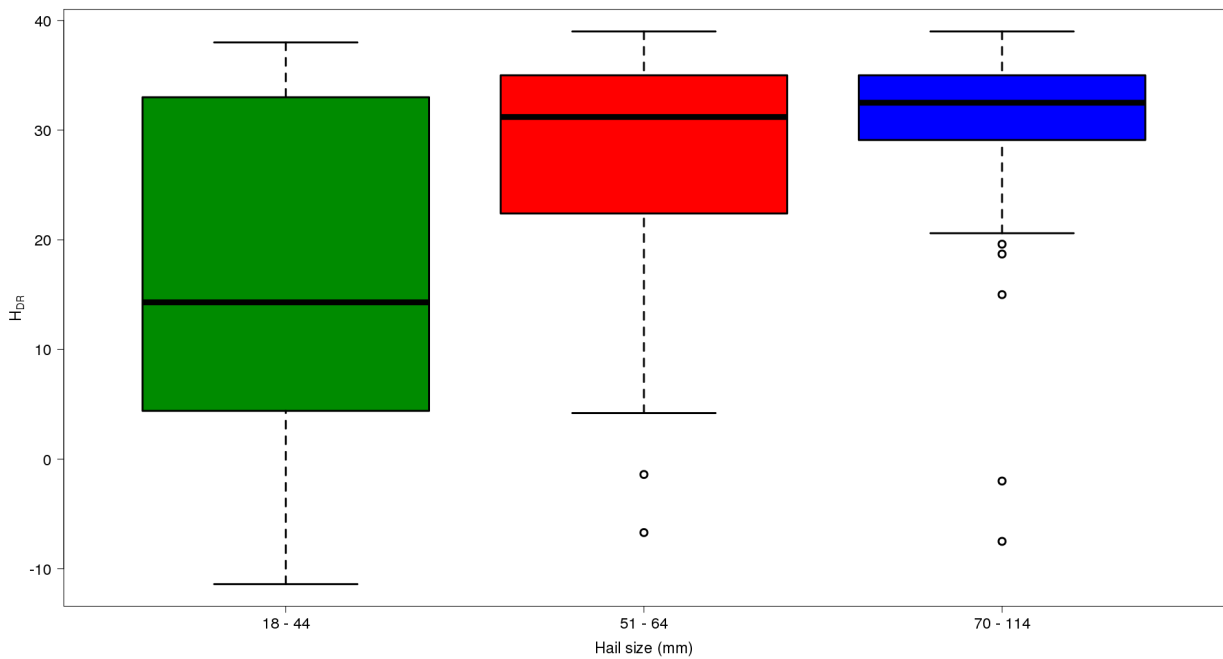


FIG. 8. Same as Fig. 5, except for  $H_{DR}$ .

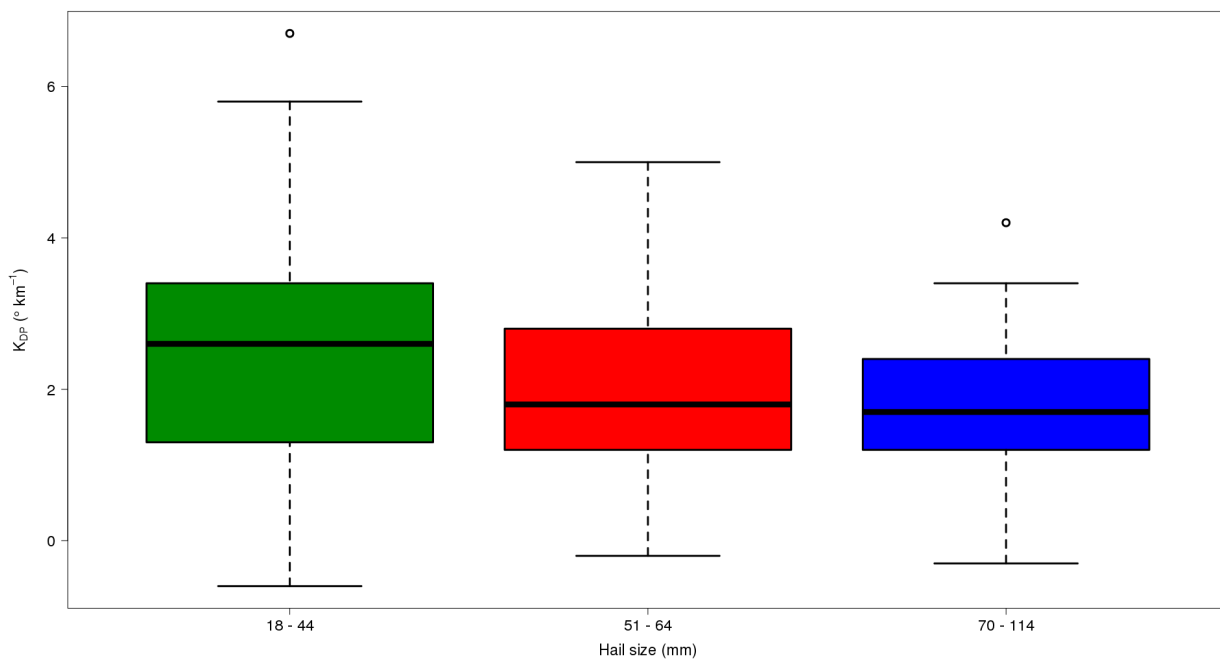


FIG. 9. Same as Fig. 5, except for  $K_{DP}$ .

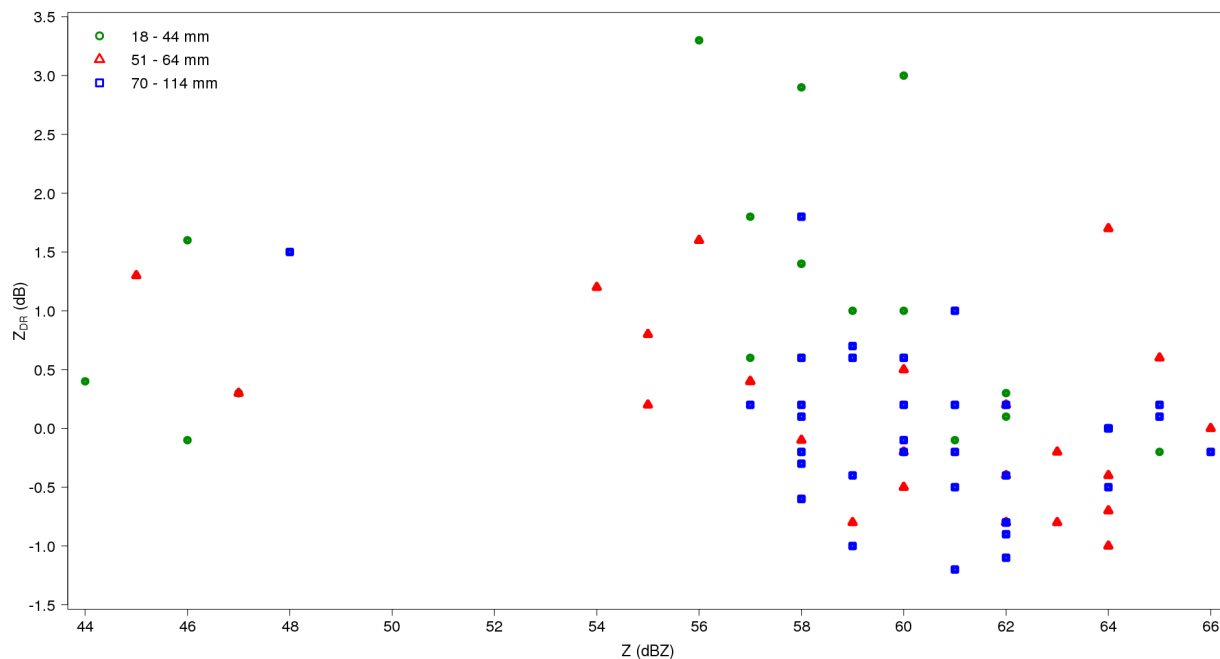


FIG. 10. Scatter plot of  $Z$  versus  $Z_{DR}$ , from the  $0.52^{\circ}$  scan for a  $1^{\circ} \times 1 \text{ km}$  window (median of eight values) centered on the location of each hail report, for three hail-size ranges.

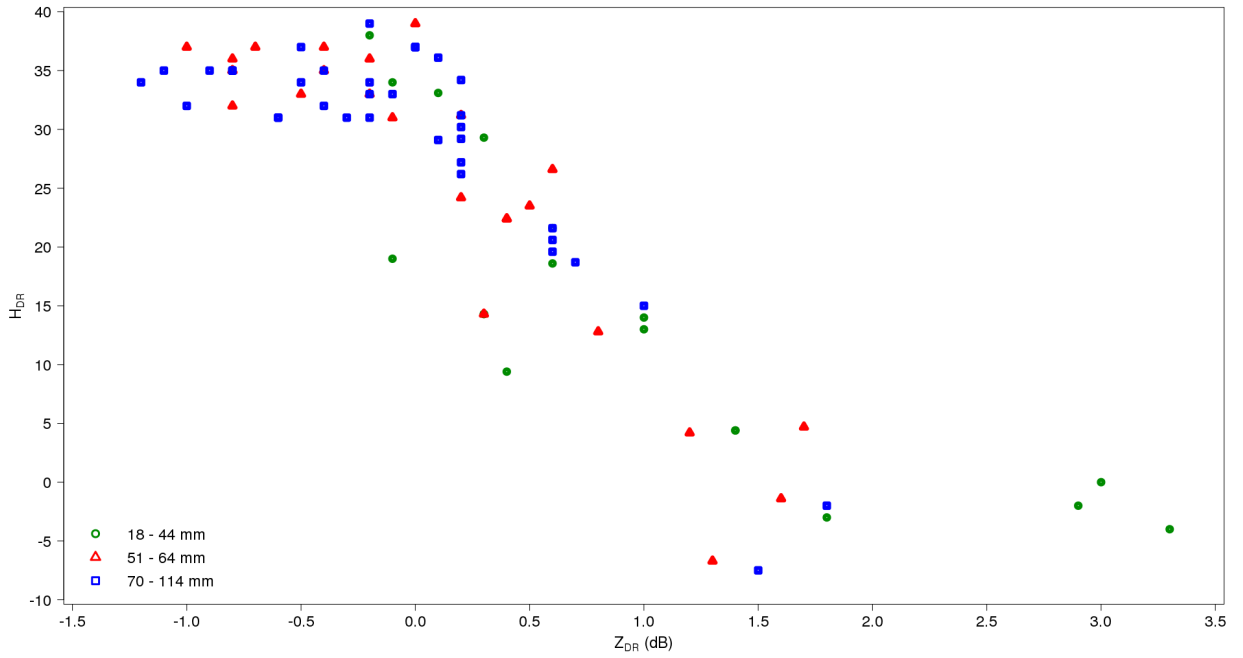


FIG. 11. Same as Fig. 10, except for  $Z_{DR}$  versus  $H_{DR}$ .

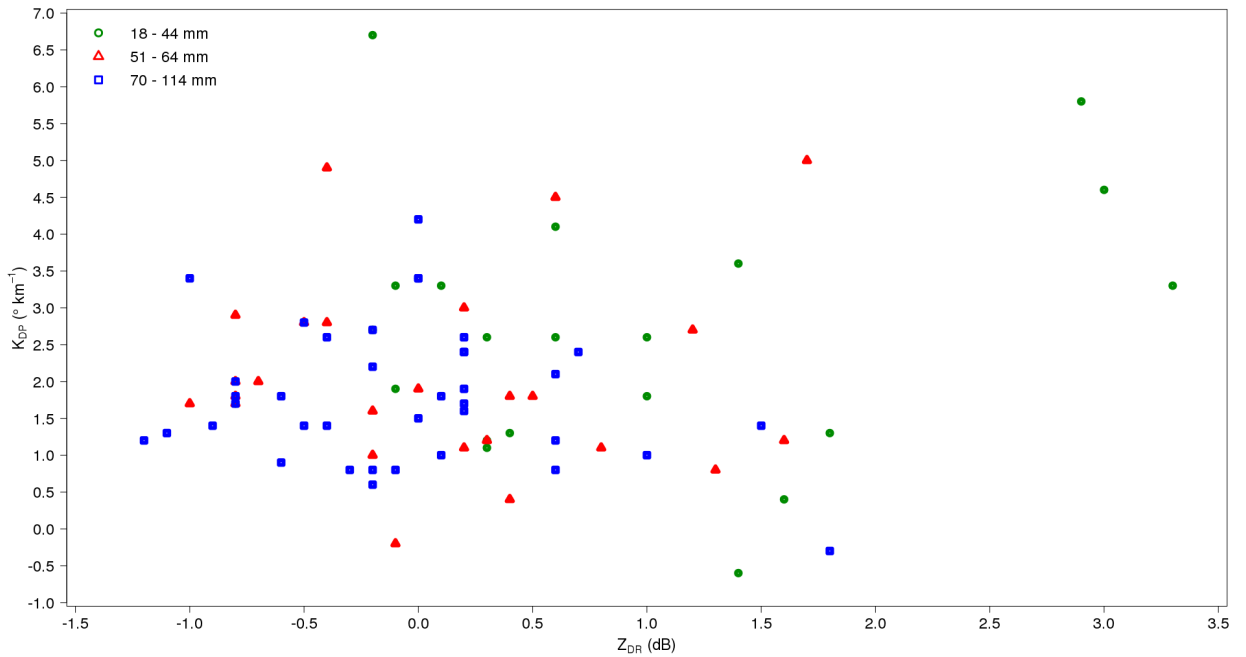


FIG. 12. Same as Fig. 10, except for  $Z_{DR}$  versus  $K_{DP}$ .

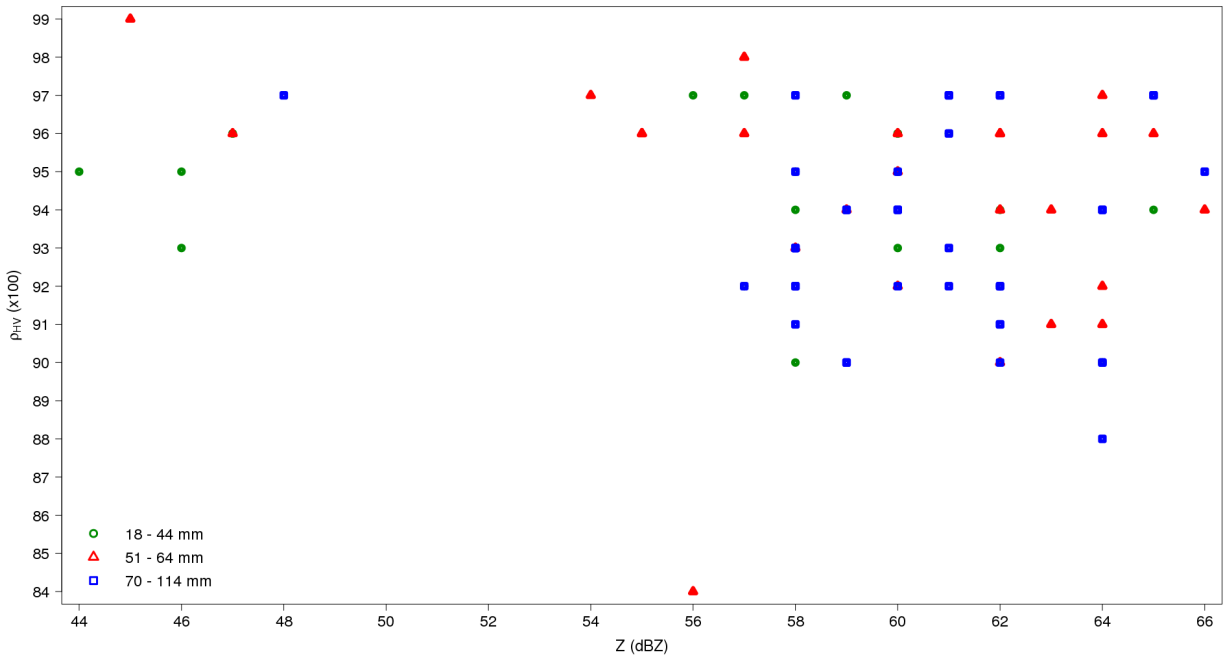


FIG. 13. Same as Fig. 10, except for Z versus  $\rho_{HV}$ .

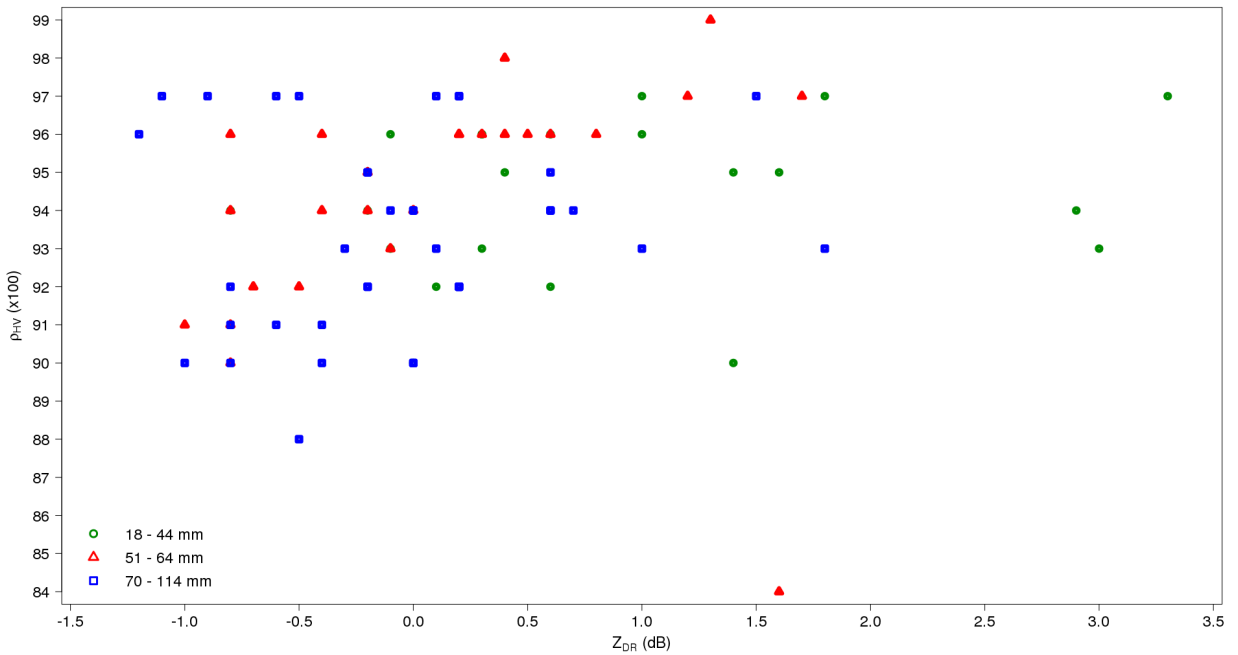


FIG. 14. Same as Fig. 10, except for  $Z_{DR}$  versus  $\rho_{HV}$ .

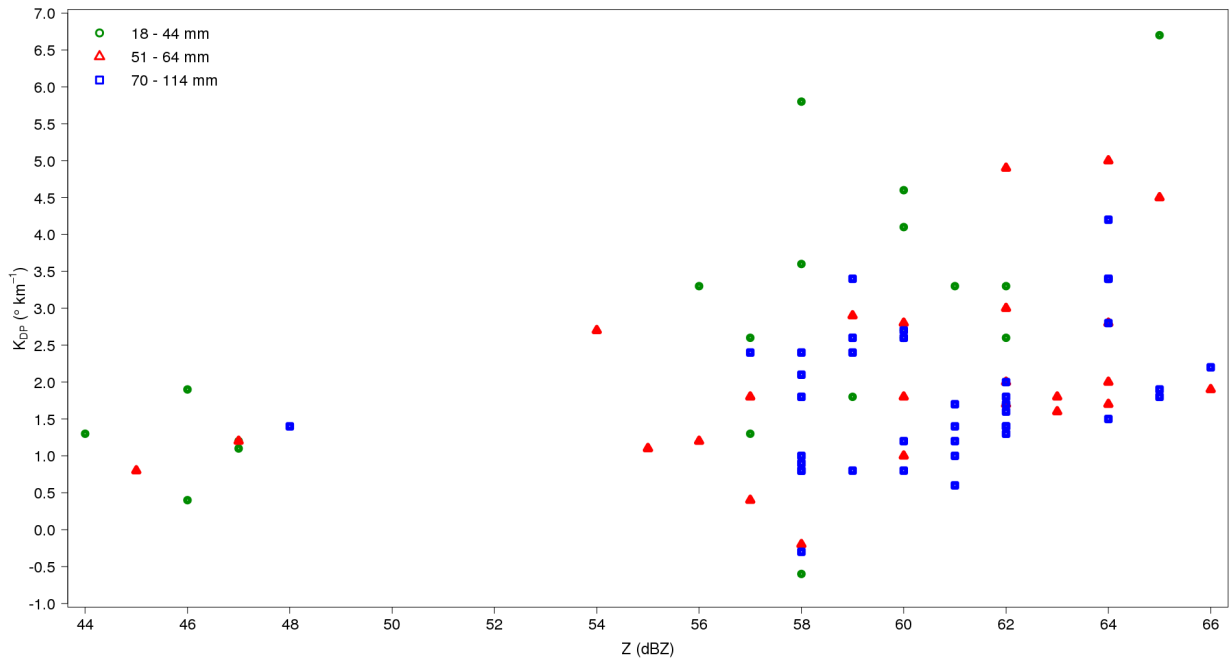


FIG. 15. Same as Fig. 10, except for Z versus  $K_{DP}$ .